NANO LETTERS

Letter

pubs.acs.org/NanoLett

Direct Temperature Mapping of Nanoscale Plasmonic Devices

Boris Desiatov,[†] Ilya Goykhman,[†] and Uriel Levy*

Department of Applied Physics, The Benin School of Engineering and Computer Science, The Center for Nanoscience and Nanotechnology, The Hebrew University of Jerusalem, Jerusalem 91904, Israel

Supporting Information

ABSTRACT: Side by side with the great advantages of plasmonics in nanoscale light confinement, the inevitable ohmic loss results in significant joule heating in plasmonic devices. Therefore, understanding optical-induced heat generation and heat transport in integrated on-chip plasmonic devices is of major importance. Specifically, there is a need for in situ visualization of electromagnetic induced thermal energy distribution with high spatial resolution. This paper studies the heat distribution in silicon plasmonic nanotips. Light is coupled to the plasmonic nanotips from a silicon nanowaveguide that is integrated with the tip on chip. Heat is generated by light absorption in the metal surrounding the silicon nanotip. The steady-state thermal distribution is studied numerically and measured experimentally using the approach of scanning thermal microscopy. It is shown that following the nanoscale heat generation by a 10 mW light source within a silicon photonic waveguide the temperature in the region of the nanotip is increased by ~15 °C compared with the ambient temperature. Furthermore, we also perform a numerical study of the dynamics of the heat transport. Given the nanoscale dimensions of the structure, significant heating is expected to occur within the time frame of picoseconds. The capability of measuring temperature distribution of plasmonic structures at the nanoscale is shown to be a powerful tool and may be used in future applications related to thermal plasmonic applications such as control heating of liquids, thermal photovoltaic, nanochemistry, medicine, heat-assisted magnetic memories, and nanolithography.

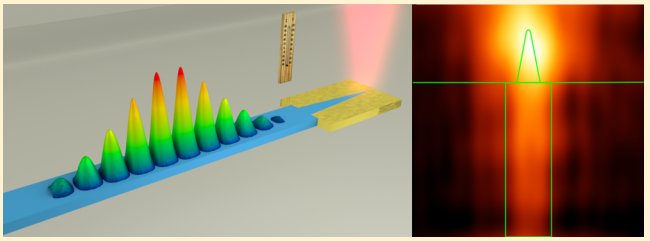

KEYWORDS: *Surface plasmons, scanning thermal microscopy, thermal imaging, nanophotonics, optical heating*

In the past two decades, nanoscale manipulation of confined electromagnetic energy in the form of surface plasmon polariton (SPP) waves residing at the boundary between metallic and dielectric layers has been studied theoretically and experimentally in great depth.[1−4] A variety of novel configurations for generating, guiding, concentrating, and detecting of SPP waves were proposed and experimentally realized. Alongside with the beneficial property of confining electromagnetic energy at the nanoscale, a major drawback of SPP waves is the inevitable high loss, that is, the electromagnetic energy is decaying as the SPP wave propagates along the metal−dielectric interface due to the high absorption in the metal. As a result of this ohmic loss, also known as a Joule heating, local heating of the SPP structure occurs.[5−7] Furthermore, owing to the strong confinement, the electromagnetic field inside the metal constituting the plasmonic structure could become very high resulting in a significant heating. Indeed, it was already shown that light-induced heat of plasmonic structures, for example, nanoparticles can be used for heating of liquids,[8,9] magnetic data storage,[10−12] microfluidics,[13−15] medicine,[16−18] and nanochemistry.[19] One of the outcomes of local heating of the plasmonic structure is the change in the refractive index of the structure via the thermooptic effect. Clearly, this may affect the properties and the functionality of the SPP devices. One of the main challenges in the field of thermal plasmonics is to directly measure the optical-induced heat with nanoscale resolution. Numerous techniques can be used for the visualization of temperature differences in micrometer and submicrometer structures including fluorescence microscopy,[20] Raman spectroscopy,[21] thermoreflectance,[22] IR microscopy,[23] fluorescence anisotropy microscopy,[24] phosphor thermometry,[25] nanodiamonds thermometry,[26] and scanning thermal microscopy (SThM).[27] These techniques are based on a variety of physical phenomena and differ in their properties, for example, in their spatial, temporal, and temperature resolution. All these techniques have advantages and disadvantages[28−30] and should be carefully selected for a specific application.

Most of the listed measuring methods are far-field techniques and thus are limited in their spatial resolution by diffraction. Overcoming the diffraction limit requires the use of other approaches, for example, operating in the near field. One of the potential candidates for achieving this goal is the SThM technique. This approach is capable of measuring thermal differences on the order of 10 mK and offering spatial resolution down to the ~10 nm range.[31] The approach has been used for thermal measurements of nanowires.[31] In this paper, we demonstrate for the first time the use of the SThM approach for the purpose of thermal imaging of plasmonic induced heating in plasmonic structures.

Received: October 17, 2013
Revised: January 8, 2014
Published: January 14, 2014

Specifically, we demonstrate the design, simulation and the thermal near field measurement by SThM of plasmonic induced heat generating within an on-chip nanoscale plasmonic focusing device constructed in an integrated silicon photonics platform. We use the silicon integrated plasmoic nanotip device[32] to obtain high confinement of electromagnetic energy at the boundary between the silicon tip and the surrounding metal. As a result, a local thermal hotspot is instantaneously generated and gradually diffused into the metal. For the purpose of this demonstration, we study a previously published plasmonic silicon nanotip with a metallic cladding that was integrated with a silicon photonic waveguides structure as shown in Figure 1. Light at the near-infrared wavelength of

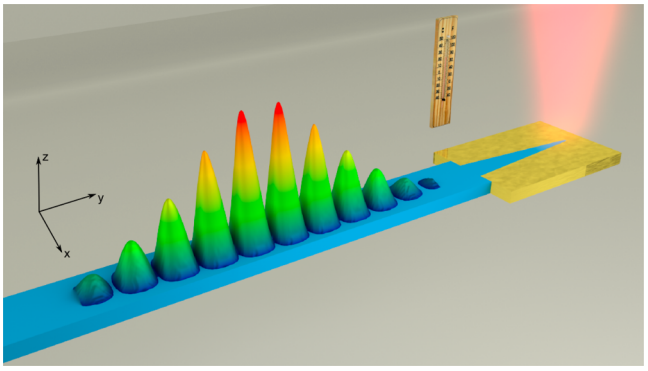

Figure 1. Schematic representation of the nanotip focusing device. The silicon photonic waveguide (blue) is coupled to a silicon tip surrounded by metal. A schematic description of an optical pulse is superimposed on the structure.

~1.5 μm is propagating along the waveguide and coupled into the metal−dielectric−metal tapered structure. As the electromagnetic energy propagates along the tapered silicon tip with metal cladding, the mode size shrinks. At the apex of the tip, the electromagnetic power is concentrated to nanoscale dimensions, resulting in high energy density. Upon interacting with the metal, the electromagnetic field decays because of the ohmic loss in the metal, and a local heat source is generated. Following the rapid generation of local heating, the thermal energy is dissipating toward the surroundings resulting in a smearing of temperature profile.

First, we investigated the optical-induced heat generation and the thermal energy distribution in the system at steady state, both numerically and experimentally. To simulate the temperature profile, we assume the excitation of the device by a continuous wave (CW) TE polarized fundamental waveguide mode with an optical power of 10 mW within a 1 μm wide, 250 nm high silicon waveguide. The waveguide is terminated by a silicon tip with a 450 nm base width, 250 nm height, 1 μm length, and 20 nm apex diameter. The tip sidewalls are surrounded by gold.

In Figure 2a, we show the simulated average electromagnetic field intensity. At the apex of the tip the electric field intensity is enhanced by a factor of ~50 compared with the electric field intensity in the waveguide. This enhanced field penetrates into the surrounding metal and serves as the source of heat. In the metal, the heat source density caused by the Joule heating is defined by $q(\bar{r}) = (\omega\varepsilon_0/2)\mathrm{Im}(\varepsilon_{\mathrm{metal}})|\bar{E}(\bar{r})|^2$. Figure 2b shows the calculated heat generation density around the dielectric tip inside the metal cladding. A significant portion of the heat generated in our structure is bounded to a nanoscale region of about 50 nm in the metallic part of the device. In Figure 2c, the steady-state temperature distribution within the structure is demonstrated. The maximum temperature rise for an input optical power of 10 mW inside the silicon waveguide was found to be 15 °C. The thermal profile of the device at steady state is broadened compared with the dimensions of the heat source due to the transport of the heat in the metal. Longitudinal and transverse profiles of Figure 2c are shown in Figure 2d.

While the above results were obtained at steady state, it should be mention that the same device can be used for the generation of an on-chip heat source with a nanometric dimensions under a femtosecond pulsed illumination. This cased is described in details by computer simulations that are provided in the Supporting Information.

Next we turn into a direct measurement of the temperature profile around the nanotip. First, we fabricated the device using a silicon-on-insulator (SOI) wafer with an upper silicon layer of 250 nm on top of a 2 μm layer of buried oxide (BOX). The silicon waveguide and the tip were defined by electron-beam (ebeam) lithography (Raith e_line 150) followed by inductive coupled plasma (ICP) reactive ion etching (RIE) (Oxford Plasmalab 100). Next, the metallic pattern was defined by an additional ebeam lithography step with high alignment accuracy. Finally, 200 nm thick gold layer was deposited on the structure, followed by a lift-off process. In Figure , a scanning electron microscope micrograph of a typical fabricated device is provided. The apex of the tip was found to be 20 nm, which is limited by our electron beam resolution.

One of the main issues related to nanoscale temperature measurements by thermocouple with nanometric dimensions is the need for a calibration process. The calibration process should determine the dependency between the measured voltage in the thermocouple and the actual temperature of the measured surface. We have chosen to use the well-known 4-probe metal line gold resistors technique[31] in order to calibrate our SThM system. The resistors were joule-heated and scanned by an atomic force microscope (AFM) (NANONICS Multi-View 4000) with a thermocouple tip for measuring the thermal signal as a function of the tip's position. The temperatures of the calibration resistors were calculated by measuring the resistivity of each resistor with 4 probe measurement technique. This calibration process takes into the account the thermocouple responsivity, the nanoscale dimensions of the measured structure and the different heat exchange processes between the sample and the thermocouple tip.

To experimentally characterize our plasmonic device we launched an in-plane polarized light (TE) at 1550 nm wavelength from a diode laser to the device by using a polarized maintained lensed fiber using "butt-coupling" technique and performed both near-field scanning microscope (NSOM) scans and SThM scans to obtain the electromagnetic field and the thermal distribution of the device. For the NSOM measurements, we used a metallic-coated NSOM tip with 250 nm aperture diameter. The thermal profiles of the device were obtained by using a thermocouple tip with 100 nm apex's diameter. The optical power within the waveguide was estimated to be ~10 mW. Figure 4a,b shows the calculated and the measured optical intensity distribution in the device. We can clearly observe a substantial concentration of electromagnetic energy in the vicinity of the apex of the tip. The difference between the simulated and the measured result can be explained by the finite resolution of our NSOm probe (250 nm aperture diameter) and by the fact that the presence

dx.doi.org/10.1021/nl403872d | Nano Lett. 2014, 14, 648−652

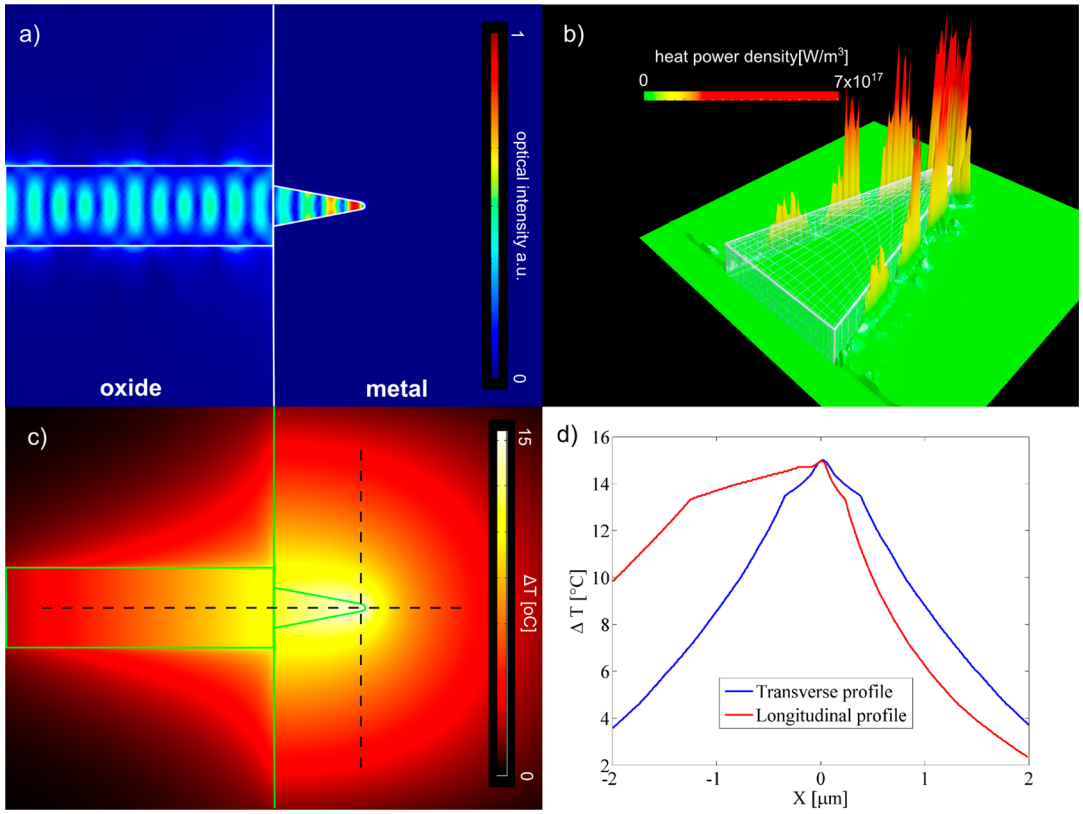

Figure 2. (a) Calculated average electromagnetic field intensity within the device. (b) Calculated heat generation density. (c) Temperature distribution around the plasmonic device at steady state. (d) Longitudinal (red) and transverse (blue) profile of heat distribution, along the dashed lines shown in panel c.

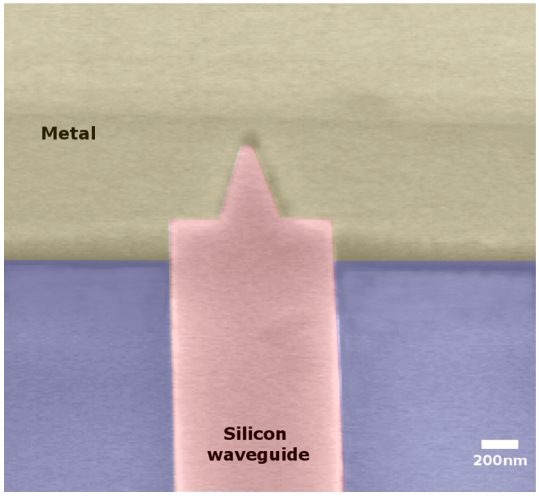

Figure 3. SEM microgrpah of a typical fabricated device.

of higher optical modes in the waveguide. Figure 4c,d shows the simulated and the measured thermal distribution in the structure. The measured maximum temperature difference was found to be ~13 °C and it is mostly confined to the area of the plasmonic nano tip, nearby the region where the optical intensity is also at its maximum. Qualitatively, the measurement agrees very nicely with the simulated result (Figure 4c). Yet, the simulated maximum temperature difference is slightly higher (~15 °C). The difference in the value of the maximal temperature can be explained by an uncertainty regarding the actual optical power in the waveguide, by the deviation of the simulated parameters (geometry, permittivity, and boundary conditions) from the actual parameters, and by the existence of higher optical modes in the waveguide.

Next, we investigate the relation between the obtained maximum temperature rise and the incident optical power. We performed several temperature scans of the device, each for a different TE polarized input optical power. In Figure 5, we plot the maximum temperature difference as a function of the input power. One can clearly observe the linear behavior of the temperature rise with the increase of the input optical power.

To emphasis the importance of the incident polarization we performed both optical and thermal scans of the studied device, this time under out of-plane (transverse magnetic, TM) polarization illumination. As for the TE case, the optical power within the waveguide is estimated to be ~10 mW. Figure 6a,b shows the optical simulation results and the NSOM scanning results for the TM polarized excitation. As can be seen, localization of the electromagnetic energy cannot be observed either in simulations or in the measurement. As a consequence of the absence of high confinement of electromagnetic energy in the vicinity of the apex, we do not anticipate a significant rise in temperature in the apex with respect to its surrounding. Indeed, this expectation is confirmed both by a numerical thermal simulation (Figure 6c) as well as by the SThM scan (Figure 6d). The maximum temperature difference in the thermal simulations and the SThM was found to be in the order of 2 °C, much lower than the heating results obtained for the case of the TE excitation.

In summary, we demonstrated the usefulness of the scanning thermal microscopy approach for the study of optically induced thermal distribution within nanoscale plasmonic structures.

dx.doi.org/10.1021/nl403872d | Nano Lett. 2014, 14, 648−652

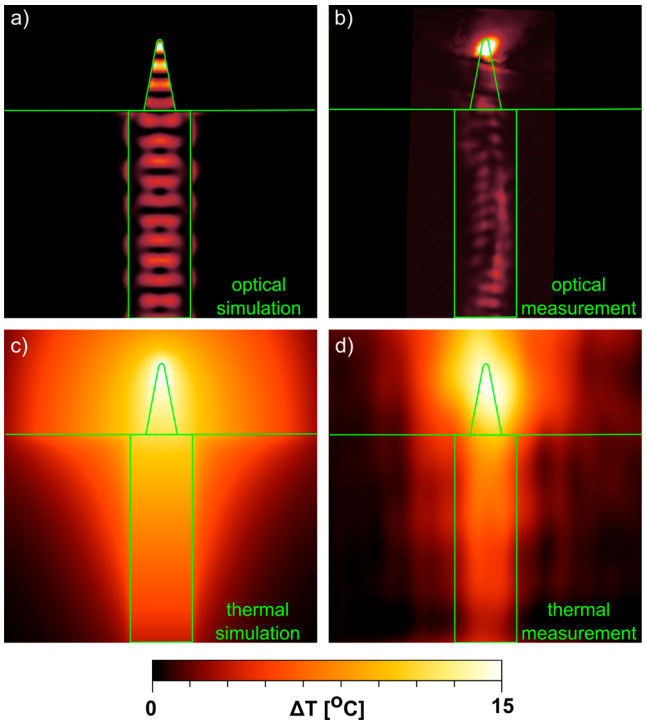

Figure 4. (a) Calculated average electromagnetic field intensity within the device. (b) NSOM measurement results showing the electromagnetic intensity distribution. (c) Simulated steady-state thermal distribution of the plasmonic nanofocusing device. (d) SThM measurement showing the temperature map of the plasmonic nanofocusing device. All results were obtained for TE polarized excitation.

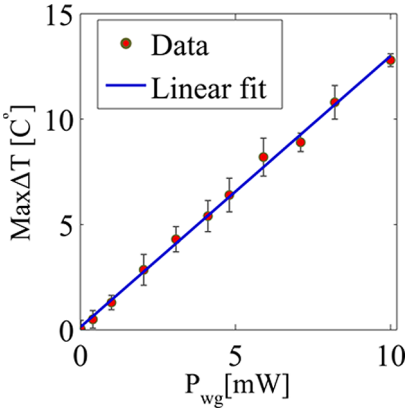

Figure 5. The measured maximal temperature rise as a function of the incident optical power. The solid line represent a linear fit to the measured data. The error bars were obtained from the difference between several (2−3) measurements.

Specifically, we observed the heat distribution in silicon plasmonic nanotips in steady state. The demonstrated device couples light from an external source and guides it through silicon waveguides into nanoscale plasmonic structures that are integrated on chip. By coupling 10 mW of optical power into the waveguide, we have observed heating of ∼15 °C at the apex of the nanotip as compared with the ambient temperature. Moreover, we have studied numerically the dynamics of heat transport in the device. Given the nanoscale dimensions of the structure, significant heating is expected to occur within a time frame of picoseconds. The demonstrated device can be used for

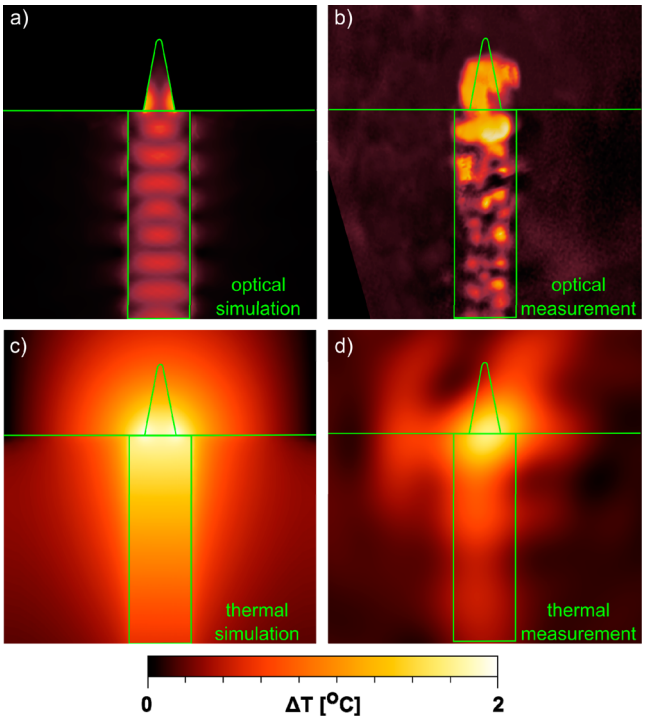

Figure 6. (a) Calculated average electromagnetic field intensity within the device. (b) NSOM measurement results showing the electromagnetic intensity distribution. (c) Simulated steady-state thermal distribution of the plasmonic nanofocusing device. (d) SThM measurement showing the temperature map of the plasmonic nanofocusing device. All results were obtained for TM polarized excitation.

providing on chip nanoscale heat sources on demand with potential applications in nanochemistry, nanomedicine, thermal photovoltaics, light detection, nanoscale fabrication, and memories. In order to further reduce the dimensions of the heat source toward the dip nanoscale, one should consider the integration of the demonstrated platform with nanoscale metallic structures (e.g., nanoantena, dimers, oligomers, and so forth).

■ ASSOCIATED CONTENT

Supporting Information

Computer simulations of the femtosecond pulse propagation, the dynamics of heat generation, and a description of simulations techniques. This material is available free of charge via the Internet at http://pubs.acs.org.

■ AUTHOR INFORMATION

Corresponding Author

*E-mail: ulevy@mail.huji.ac.il.

Author Contributions

†B.S. and I.G. contributed equally to this work.

Notes

The authors declare no competing financial interest.

■ ACKNOWLEDGMENTS

The research was supported in parts by the U.S-Israel binational science foundation, and the Israeli Science Foundation. Boris Desiatov and Ilya Goykhman acknowledges the Eshkol fellowship from the Israeli Ministry of Science and Technology. The devices were fabricated at the Center for

Nanoscience and Nanotechnology, The Hebrew University of Jerusalem.

REFERENCES

(1) Schuller, J. A.; Barnard, E. S.; Cai, W.; Jun, Y. C.; White, J. S.; Brongersma, M. L. *Nat. Mater.* **2010**, *9*, 193−204.
(2) Stockman, M. I. *Opt. Express* **2011**, *19*, 22029−22106.
(3) Novotny, L.; van Hulst, N. *Nat. Photonics* **2011**, *5*, 83−90.
(4) Gramotnev, D. K.; Bozhevolnyi, S. I. *Nat Photonics* **2010**, *4*, 83−91.
(5) Govorov, A. O.; Richardson, H. H. *Nano Today* **2007**, *2*, 30−38.
(6) Baffou, G.; Quidant, R.; Girard, C. *Appl. Phys. Lett.* **2009**, *94*, 153109.
(7) Baffou, G.; Quidant, R. *Laser Photonics Rev.* **2012**, DOI: 10.1002/lpor.201200003.
(8) Fang, Z.; Zhen, Y.-R.; Neumann, O.; Polman, A.; García de Abajo, F. J.; Nordlander, P.; Halas, N. J. *Nano Lett.* **2013**, *13*, 1736−1742.
(9) Neumann, O.; Urban, A. S.; Day, J.; Lal, S.; Nordlander, P.; Halas, N. J. *ACS Nano* **2012**, *7*, 42−49.
(10) Stipe, B. C.; et al. *Nat. Photonics* **2010**, *4*, 484−488.
(11) Xu, B. X.; Liu, Z. J.; Ji, R.; Toh, Y. T.; Hu, J. F.; Li, J. M.; Zhang, J.; Ye, K. D.; Chia, C. W. *J. Appl. Phys.* **2012**, *111*, 07B701+.
(12) Challener, W. A.; Peng, C.; Itagi, A. V.; Karns, D.; Peng, W.; Peng, Y.; Yang, X.; Zhu, X.; Gokemeijer, N. J.; Hsia, Y. T.; Ju, G.; Rottmayer, R. E.; Seigler, M. A.; Gage, E. C. *Nat. Photonics* **2009**, *3*, 220−224.
(13) Donner, J. S.; Baffou, G.; McCloskey, D.; Quidant, R. *ACS Nano* **2011**, *5*, 5457−5462.
(14) Wang, K.; Schonbrun, E.; Steinvurzel, P.; Crozier, K. B. *Nat. Commun.* **2011**, *2*, 469.
(15) Liu, G. L.; Kim, J.; Lu, Y.; Lee, L. P. *Nat. Mater.* **2006**, *5*, 27−32.
(16) Gobin, A. M.; Lee, M. H.; Halas, N. J.; James, W. D.; Drezek, R. A.; West, J. L. *Nano Lett.* **2007**, *7*, 1929−1934.
(17) Han, G.; Ghosh, P.; De, M.; Rotello, V. M. *Nanobiotechnology* **2007**, *3*, 40−45.
(18) Jain, P. K.; El-Sayed, I. H.; El-Sayed, M. A. *Nano Today* **2007**, *2*, 18−29.
(19) Cao, L.; Barsic, D. N.; Guichard, A. R.; Brongersma, M. L. *Nano Lett.* **2007**, *7*, 3523−3527.
(20) Donner, J. S.; Thompson, S. A.; Alonso-Ortega, C.; Morales, J.; Rico, L. G.; Santos, S. I. C. O.; Quidant, R. *ACS Nano* **2013**, *7* (10), 8666−8672.
(21) Liu, K.-L. K.; Davis, K. L.; Morris, M. D. *Anal. Chem.* **1994**, *66*, 3744−3750.
(22) Baffou, G.; Bon, P.; Savatier, J.; Polleux, J.; Zhu, M.; Merlin, M.; Rigneault, H.; Monneret, S. *ACS Nano* **2012**, *6*, 2452−2458.
(23) Kondo, S.; Hinode, K. *Appl. Phys. Lett.* **1995**, *67*, 1606−1608.
(24) Baffou, G.; Kreuzer, M. P.; Kulzer, F.; Quidant, R. *Opt. Express* **2009**, *17*, 3291−3298.
(25) Coppens, Z. J.; Li, W.; Walker, D. G.; Valentine, J. G. *Nano Lett.* **2013**, *13*, 1023−1028.
(26) Kucsko, G.; Maurer, P. C.; Yao, N. Y.; Kubo, M.; Noh, H. J.; Lo, P. K.; Park, H.; Lukin, M. D. *Nature* **2013**, *500*, 54−58.
(27) Williams, C. C.; Wickramasinghe, H. K. *Appl. Phys. Lett.* **1986**, *49*, 1587−1589.
(28) Christofferson, J.; Maize, K.; Ezzahri, Y.; Shabani, J.; Wang, X.; Shakouri, A. *J. Electron. Packag.* **2008**, *130*, 041101+.
(29) Kölzer, J.; Oesterschulze, E.; Deboy, G. *Microelectron. Eng.* **1996**, *31*, 251−270.
(30) Yue, Y.; Wang, X. *Nano Rev.* **2012**, 3.
(31) Kim, K.; Chung, J.; Hwang, G.; Kwon, O.; Lee, J. S. *ACS Nano* **2011**, *5*, 8700−8709.
(32) Desiatov, B.; Goykhman, I.; Levy, U. *Opt. Express* **2011**, *19*, 13150−13157.